ADVANCING EARTH AND SPACE SCIENCES

AGU Advances

RESEARCH ARTICLE
10.1029/2025AV001654

# Role of ULF Waves in Reforming the Martian Bow Shock

**Chi Zhang[1], Chuanfei Dong[1], Terry Z. Liu[2], Christian Mazelle[3], Savvas Raptis[4], Hongyang Zhou[1], Jacob Fruchtman[5], Jasper Halekas[5], Jing-Huan Li[6], Kathleen G. Hanley[7], Shannon M. Curry[8], David L. Mitchell[7], and Xinmin Li[1]**

[1]Center for Space Physics and Department of Astronomy, Boston University, Boston, MA, USA, [2]Department of Earth, Planetary, and Space Sciences, University of California, Los Angeles, CA, USA, [3]IRAP, Université de Toulouse, CNRS, UPS, CNES, Toulouse, France, [4]Johns Hopkins University Applied Physics Laboratory, Laurel, MD, USA, [5]Department of Physics and Astronomy, University of Iowa, Iowa City, IA, USA, [6]Swedish Institute of Space Physics, Uppsala, Sweden, [7]Space Sciences Laboratory, University of California, Berkeley, CA, USA, [8]Laboratory for Atmospheric and Space Physics, University of Colorado, Boulder, CO, USA

**Peer Review** The peer review history for this article is available as a PDF in the Supporting Information.

**Key Points:**

- The reformation of the Martian bow shock exhibits distinctive characteristics that set it apart from those observed at other planets
- Shock reformation driven by ultra-low frequency (ULF) waves at Mars is less dependent on shock geometry compared to other planets
- ULF waves periodically modulate the local shock geometry, thereby influencing the motion of reflected ions

**Supporting Information:**

Supporting Information may be found in the online version of this article.

**Correspondence to:**

C. Zhang and C. Dong,
zc199508@bu.edu;
dcfy@bu.edu

**Citation:**

Zhang, C., Dong, C., Liu, T. Z., Mazelle, C., Raptis, S., Zhou, H., et al. (2025). Role of ULF waves in reforming the Martian bow shock. *AGU Advances*, *6*, e2025AV001654. https://doi.org/10.1029/2025AV001654

Received 27 JAN 2025
Accepted 30 JUN 2025

**Author Contributions:**

**Conceptualization:** Chi Zhang
**Data curation:** Kathleen G. Hanley, David L. Mitchell
**Formal analysis:** Chi Zhang, Terry Z. Liu
**Funding acquisition:** Chuanfei Dong, Shannon M. Curry
**Investigation:** Terry Z. Liu
**Methodology:** Chi Zhang
**Software:** Chi Zhang
**Supervision:** Chuanfei Dong



**Abstract** Understanding the nature of planetary bow shocks is beneficial for advancing our knowledge of solar wind interactions with planets and fundamental plasma physics processes. Here, we utilize data from the Mars Atmosphere and Volatile Evolution (MAVEN) spacecraft to investigate the Martian bow shock, revealing its distinctive characteristics within our solar system. We find that unlike other planetary shocks, the reformation of Mars's bow shock driven by the ultra-low frequency (ULF) waves is more global and less dependent on shock geometries. This distinct behavior is attributed to the broad distribution of ULF waves in the upstream region at Mars, generated not only by shock-reflected ions but also by planetary protons. Additionally, during the reformation process, the amplitude of the ULF waves and the steepened structures are significantly large. This results in the newly reformed shock exceeding the original one, a phenomenon not observed at other planets under similar shock conditions. Therefore, the ULF waves significantly enhance the complexity of shock dynamics and play a more substantial role at Mars compared to other planets.

**Plain Language Summary** The Sun continuously emits a high-speed plasma flow into interplanetary space, known as the solar wind. When this solar wind encounters Mars, a bow shock forms in front of Mars, decelerating and heating the incoming solar wind. This bow shock plays a pivotal role in mediating interactions between the solar wind and Mars. The bow shock may undergo cyclical reformations, meaning that the shock is periodically re-established over time. In this study, we utilize observations from spacecraft to study the Martian bow shock reformation. We discovered that the reformation processes of the Martian bow shock exhibit distinctive characteristics not seen at other planets. Specifically, we show that shock reformation, typically restricted to only parts of the shock at other planets, may occur throughout the entire Martian bow shock and under a wider range of conditions. Our findings suggest that the Martian bow shock serves as an uniquely valuable laboratory for studying shock phenomena and the underlying fundamental plasma physics.

## 1. Introduction

Collisionless shocks are fundamental and ubiquitous structures in space and astrophysical plasma environments. These shocks enable significant energy conversion between electromagnetic fields and particles, serving as sites for particle acceleration (e.g., Burgess et al., 2012; Burgess & Scholer, 2015; Liu et al., 2019). Acting as the initial barrier against the solar wind, the planetary bow shocks significantly decelerates the supersonic solar wind and heats it, providing a natural laboratory for exploring shock physics. Thus, studying the planetary bow shock not only advances our understanding of fundamental plasma physics but also enriches our insights into the interactions between the solar wind and planets.

The high Mach number of the incident solar wind necessitates that the bow shock reflects a portion of solar wind to dissipate energy (e.g., Gosling et al., 1982; Paschmann et al., 1982). This reflection may be either specular or nonspecular, depending on the ratio between the energy of the incident solar wind and the cross-shock electrostatic potential (Balikhin & Gedalin, 2022; Khotyaintsev et al., 2024). Based on the shock normal angle, $\theta_{Bn}$, defined as the angle between the upstream magnetic field and the shock normal (e.g., Schwartz et al., 1983), shocks are categorized into quasi-parallel shocks ($\theta_{Bn} < 45°$) and quasi-perpendicular ($\theta_{Bn} > 45°$) shocks. When the $\theta_{Bn}$ is close to 45°, the shock is in an intermediate state between these two regimes, termed oblique shock. In

**Validation:** Christian Mazelle, Savvas Raptis, Hongyang Zhou, Jacob Fruchtman
**Visualization:** Xinmin Li
**Writing – original draft:** Chi Zhang
**Writing – review & editing:** Chuanfei Dong, Terry Z. Liu, Christian Mazelle, Savvas Raptis, Hongyang Zhou, Jacob Fruchtman, Jasper Halekas, Jing-Huan Li, Kathleen G. Hanley, Xinmin Li

quasi-perpendicular shocks, the reflected ions predominantly engage in cyclotron motion, limiting their upstream travel to approximately 1–2 gyroradii (Balikhin & Gedalin, 2022; Sckopke et al., 1983). Conversely, the quasi-parallel shock is magnetically connected to the upstream region, allowing reflected ions to travel further upstream and have strong interactions with the incoming solar wind. These interactions lead to the generation of various types of plasma waves and transient structures (e.g., Collinson et al., 2023; Eastwood, Lucek, et al., 2005; Madanian et al., 2023; Zhang, Dong, Zhou, Halekas, et al., 2025).

The bow shock can be nonstationary, undergoing cyclical reformations or exhibiting ripples on the shock plane (e.g., Lefebvre et al., 2009; Li et al., 2024; Liu et al., 2021). Previous studies have shown that the reformation process of the terrestrial bow shock depends on its geometry. In the reformation of quasi-parallel shocks or oblique shocks that are very close to quasi-parallel shocks, it is observed that the amplitude of ULF waves generated by reflected ions increases as they approach the shock (Johlander et al., 2022; Lefebvre et al., 2009; Raptis et al., 2022). These waves then nonlinearly steepen, evolving into short large-amplitude magnetic structures (SLAMS) or other nonlinearly steepened waves (e.g., Shocklets). As they approach the bow shock, the amplitude of these nonlinear structures becomes comparable to that of the main shock, eventually replacing it and driving the reformation of quasi-parallel shocks. Regarding the oblique shocks, ULF waves can also trigger the reformation by modulating the upstream conditions (Liu et al., 2021). In contrast, quasi-perpendicular shocks can undergo self-reformation, driven by the periodic formation of new ramps created by reflected ions in the foot region (Mazelle & Lembège, 2021; Yang et al., 2020). This process is commonly known as self-reformation. These shock reformation processes are universal and applicable to other planets as well. Sundberg et al. (2013) reported that the reformation process can also occur in Mercury's quasi-parallel shock. Sulaiman et al. (2015) observed that Saturn's quasi-perpendicular shock can undergo self-reformation as well. Despite occurring on different planets, these reformation processes closely resemble those observed in Earth's bow shock. In addition to shock geometry, the Mach number also plays an important role in influencing shock dynamics. SLAMS and high-amplitude ULF waves are more likely to occur in high Mach number shocks (Bergman et al., 2025; Collinson et al., 2023; Karlsson et al., 2024; Kajdič et al., 2021; Madanian et al., 2021).

Although Mars lacks a global dipole magnetic field, the interaction between Mars and the external solar wind generates an induced magnetosphere and bow shock (e.g., Fruchtman et al., 2023; Gruesbeck et al., 2018; Zhang, Rong, et al., 2022; Zhang, Dong, Zhou, Deca, et al., 2025b). The Martian bow shock is uniquely characterized within the solar system by several factors. Firstly, Mars's neutral exosphere, particularly the hydrogen exosphere, can extend beyond 10 Mars radii ($R_M$, which is 3,390 km) due to the planet's low gravity (e.g., Chaffin et al., 2015). This extension surpasses the bow shock, whose standoff distance is typically less than 2 $R_M$. These neutral exospheric particles may become ionized, transforming into planetary protons. Similar to shock-reflected ions, these planetary protons interact with the incident solar wind, generating ULF waves in the upstream region through ion/ion beam instability (e.g., Gary, 1991; Delva et al., 2011). As the planetary protons mainly move perpendicular to the background magnetic field with negligible parallel velocity, the observed frequency of such ULF waves should be close to the proton gyrogrequency (Delva et al., 2011). In this case, these ULF waves are generally referred to as proton cyclotron waves (PCWs, Bertucci et al., 2013; Liu et al., 2020; Romanelli et al., 2016, 2018). While the foreshock ULF waves driven by reflected ions are confined to the foreshock region, PCWs can occur in both foreshock and non-foreshock regions. Consequently, the upstream region of Mars is pervaded by ULF waves, independent of the shock geometry. Second, the Martian bow shock not only reflects the incident solar wind (Barabash & Lundin, 1993; Richer et al., 2012; Yamauchi et al., 2011, 2012) but can also reflect pickup planetary heavy ions, potentially forming a heavy ion foreshock (Masunaga et al., 2016; Yamauchi, Lundin et al., 2015; Yamauchi, Hara et al., 2015). Third, the spatial scale of bow shock at Mars is comparable to the gyroradius of upstream ions, implying that kinetic effects and shock curvature may play a significant role (Madanian et al., 2023). Additionally, Shan et al. (2020) suggested that quasi-perpendicular shocks on Mars could potentially be formed by the steepening of upstream ULF waves, indicating distinctive formation mechanisms compared to other planets. Given these factors, the Martian bow shock is anticipated to be more dynamic and complex compared to the bow shocks observed on other planets (e.g., Mazelle et al., 2004). Recently, Madanian et al. (2020) reported a case of self-reformation of quasi-perpendicular shock at Mars, which is consistent with those observed on Earth and other planets. Nonetheless, our understanding of shock dynamics at Mars remains limited due to the scarcity of studies.

In this study, utilizing measurements from MAVEN (Jakosky et al., 2015), we investigate the reformation of the oblique or quasi-perpendicular bow shock at Mars. We show that the shock reformation at Mars differs from that observed in the bow shocks of other planets. This difference is primarily attributed to the widespread distribution of ULF waves generated by newly ionized planetary ions.

## 2. Data Sets and Methods

We employ magnetic field data from the Magnetometer (Connerney et al., 2015), ion measurements from the Solar Wind Ion Analyzer (SWIA) instrument (Halekas et al., 2015) and the Suprathermal and Thermal Ion Composition (STATIC) instrument (McFadden et al., 2015), along with electron data from the SolarWind Electron Analyzer (SWEA) (Mitchell et al., 2016) onboard MAVEN.

To accurately determine the plasma moment of solar wind ions, we adopt the methodology outlined by Burne et al. (2021). For the upstream region, we utilize the full ion distributions from SWIA fine measurements. In the transition and downstream regions, we apply the full ion distributions from SWIA coarse measurements. We then employ the integral method to calculate the moments, including density and velocity, as detailed by Zhang, Futaana, et al. (2022).

## 3. Observations

The analyzed shock event is part of the database provided by Fruchtman et al. (2023). It occurred between 00:30 and 01:00 UTC on 7 January 2017, as the MAVEN spacecraft transitioned from the upstream solar wind into the downstream magnetosheath (see Figures 1a and 1b). Figures 1c–1h provide an overview of the shock event. Before 00:39:30 UTC (see the red shaded interval in Figure 1), MAVEN was in the upstream region, where it consistently detected a weak magnetic field (Figure 1c), unshocked solar wind electrons (Figure 1d), and ions (Figure 1e). The STATIC measurements show that only protons ($H^+, m/q = 1$) and helium ions ($He^{++}, m/q = 2$) are involved in this case (see Figure 1f), both of which are typical of the solar wind. There is no clear evidence of planetary heavy ions. Between 00:39:30 and 00:48:45 UTC, corresponding to the green shaded interval in Figure 1, MAVEN recorded a significant enhancement in magnetic field strength, along with the compression and deceleration of solar wind ions (Figures 1g and 1h), marking its entry into the shock transition region. After 00:48:45 UTC, as shown in the gray shaded interval, the magnetic field strength and solar wind velocity stabilized, accompanied by heating of electrons and ions (see Figures 1d and 1e), indicating that MAVEN had entered the downstream magnetosheath region.

We calculated the average parameters for the upstream and downstream regions, as presented in Table 1. Using these parameters, we determine the shock normal direction based on the mixed-mode coplanarity method (Schwartz, 1998), yielding a normal vector of (0.79, 0.245, 0.56). This outcome aligns closely with the bow shock model proposed by Trotignon et al. (2006), which gives a vector of (0.62, 0.3, 0.72), differing by an angular measure of approximately 13.8°. Similarly, it corresponds well with the results from Fruchtman et al. (2023), which is (0.766, 0.32, 0.555). The estimated shock normal angle, $\theta_{Bn}$, is about 51.59°, which is close to 45°. Consequently, we classify this as an oblique shock. Table 1 also reveals that the Alfvén Mach number ($M_A$) of the analyzed shock is 6.03, which is lower than typical conditions, usually ranging between 10 and 20 (Halekas et al., 2023).

### 3.1. ULF Waves, SLAMS and Shock Reformation

The magnetic fields clearly display periodic variations in the upstream region (see Figure 2a), indicating the presence of ULF waves. These ULF waves have a frequency of 0.04 Hz, closely aligning with the proton gyrofrequency ($f_{H^+}$) of approximately 0.047 Hz, as illustrated in Figures 2b and 2e. The wave normal angle (the angle between the wave vector and the background magnetic field) of the ULF waves is less than 40° (see Figure 2c), suggesting quasi-parallel progapation. The ellipticity of the ULF waves is approximately −0.6, indicating that the waves are left-handed polarized in the spacecraft frame (see Figure 2d). Moreover, Figure 2e shows that the ULF waves are dominated by the transverse fluctuations. These characteristics align with those of either foreshock ULF wave (Eastwood, Balogh, et al., 2005), or PCWs. Given that this case occurred at an oblique shock and near perihelion at a solar longitude (Ls) of 295°, where foreshock ULF waves are not expected but PCWs are more prevalent (Andrés et al., 2025; Romanelli et al., 2016), these waves are more likely to be PCWs generated by pickup ions. The absence of observed planetary heavy ions does not contradict this interpretation, as the PCWs are initiated by pickup planetary protons. If we assume that the observed ULF waves propagated toward the upstream region at the local Alfven velocity in the plasma frame, which is about 50 km/s (Eastwood,

10.1029/2025AV001654

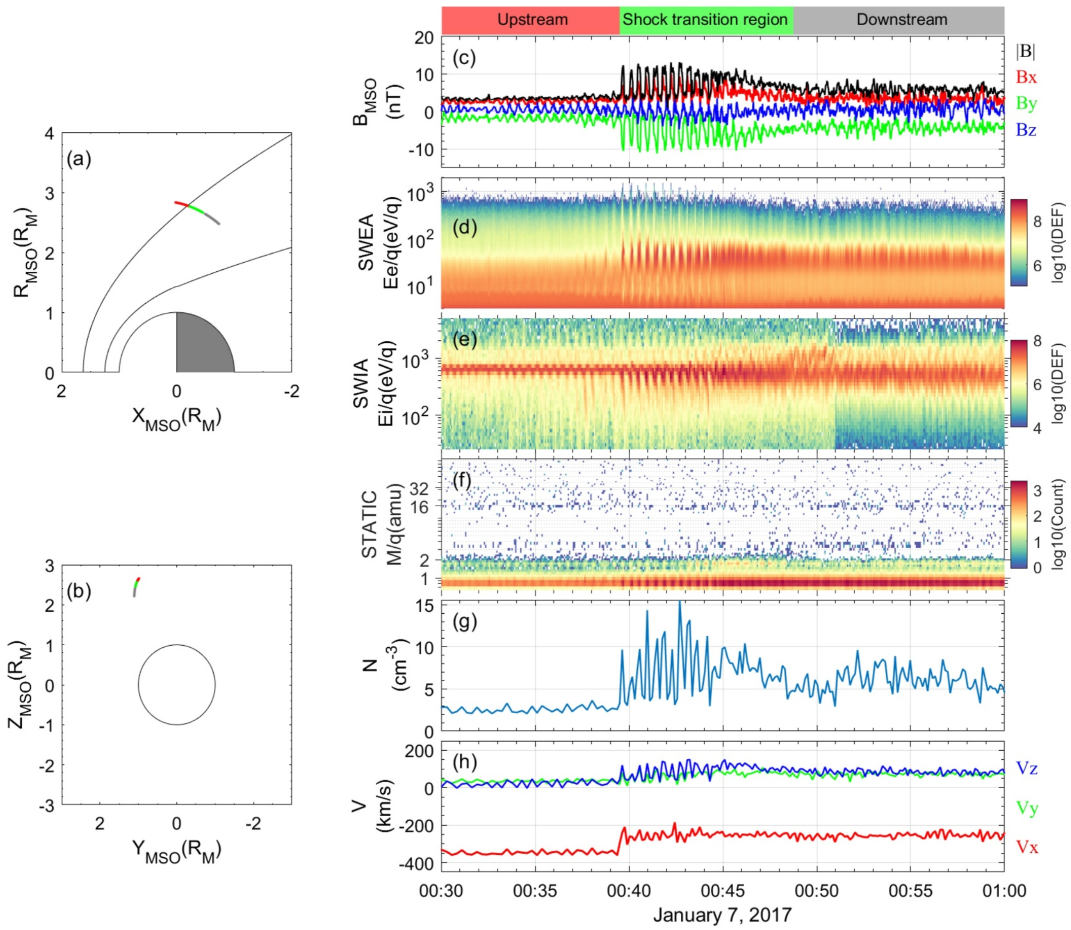


**Figure 1.** Overview of the bow shock event occurred in 00:30–01:00 UTC, January 7, 2017. (a) Shows the location of the observed events in the $X_{\mathrm{MSO}} - R_{\mathrm{MSO}}$ plane, where $R = \sqrt{Y_{\mathrm{MSO}}^2 + Z_{\mathrm{MSO}}^2}$. The overlaid curves represent the nominal bow shock and the magnetic pile-up boundary (Trotignon et al., 2006). (b) Shows the location in the $Y_{\mathrm{MSO}} - Z_{\mathrm{MSO}}$ plane. The different colors in panels (a, b) correspond to the regions as outlined at the top of panel (c). (c): Magnetic fields. (d): Electron energy spectrum. (e): Ion energy spectrum. (f): Ion mass spectrum. (g): Ion number density. (h): Ion bulk velocity.

**Table 1**
*Shock Parameters*

| Region | Parameter | Value |
|---|---|---|
| Upstream (00:20–00:25) | Density ($n_u$) | 2.35 cm$^{-3}$ |
| | Magnetic field ($\vec{B}_u$) | (2.52, −1.66, 0.57) nT |
| | Velocity ($\vec{V}_u$) | (-352.64, 32.7, 8.31) km/s |
| Downstream (00:55–01:00) | Density ($n_d$) | 5.85 cm$^{-3}$ |
| | Magnetic field ($\vec{B}_d$) | (3.23, −4.3, 0.72) nT |
| | Velocity ($\vec{V}_d$) | (-253.5, 70.69, 82.07) km/s |
| Shock | Normal vector ($\vec{n}$) | (0.79, 0.245, 0.56) |
| | Shock normal angle ($\theta_{\mathrm{Bn}}$) | 51.59° |
| | Alfvén Mach number ($M_A$) | 6.03 |

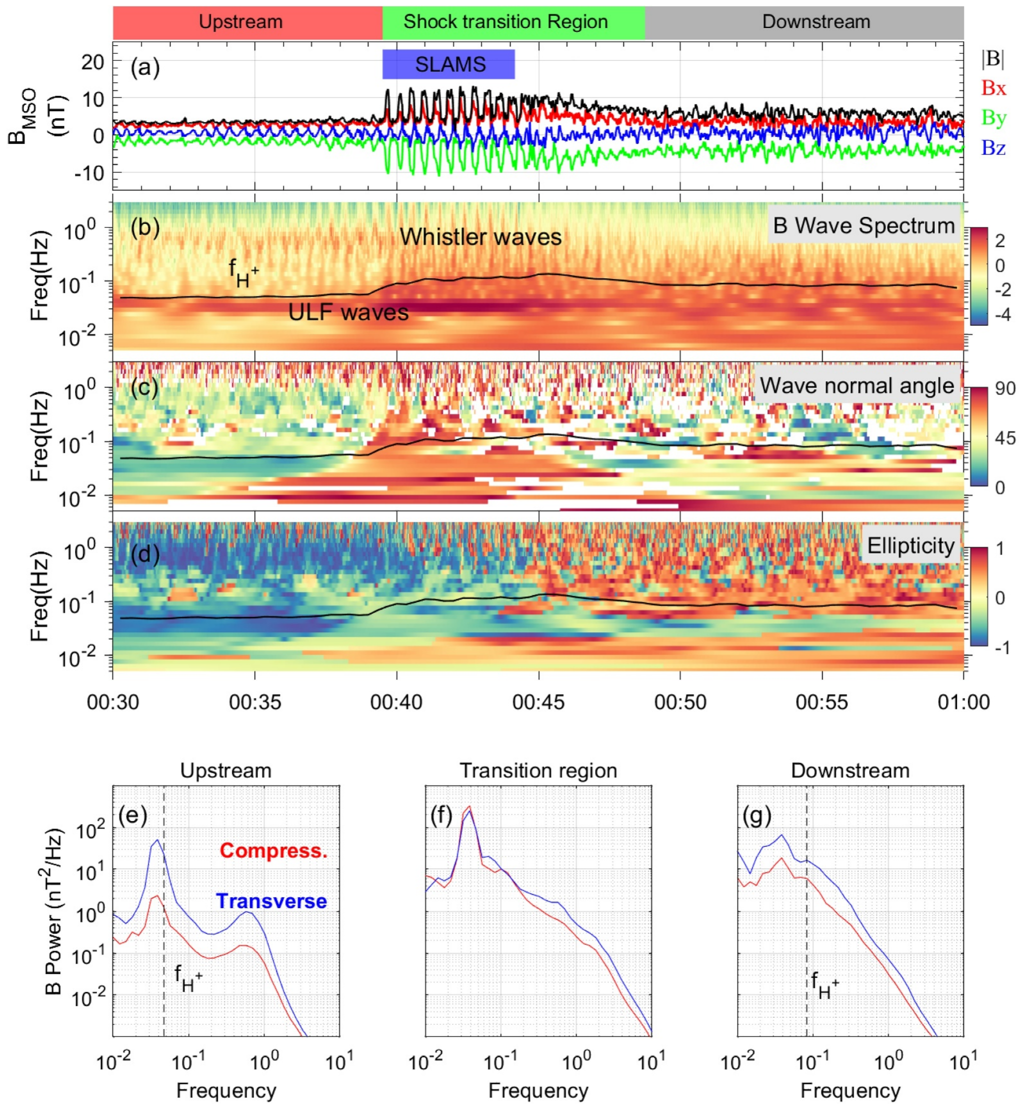


**Figure 2.** (a) Magnetic fields. (b) Magnetic field power spectrum. (c) Wave normal angle. (d) Ellipticity of the waves. The black curves in panels (b–d) represent the local proton gyrofrequency. Panels (e–g) show the power spectral density of transverse (blue) and compressive (red) magnetic field components in the upstream, transition, and downstream regions, respectively.

Balogh, et al., 2005), then in the spacecraft frame, the propagation speed of the ULF waves would be approximately 310 km/s. Given the period of the ULF waves is roughly 25 s, the wavelength can be estimated as 7,750 km (∼2 $R_M$ or 7 times of the local proton gyroradius). This suggests that the observed ULF waves are generated far away from the shock, where the reflected ions are unlikely to reach in the case of an oblique shock. Therefore, it is more plausible that the observed ULF waves are generated by planetary protons, which are formed from the ionization of neutral particles in the extended hydrogen exosphere. However, identifying pickup protons remains challenging, as their flux is relatively low compared to that of reflected ions, and the two ion populations are mixed. In addition to the ULF waves, we can also observe a high-frequency wave at a frequency of 0.8 Hz in the upstream region (Figure 2b). These waves are commonly referred to as 1 Hz waves and frequently observed near the shock (Ruhunusiri et al., 2018).

In the shock transition region, MAVEN detected periodic large-amplitude structures in the magnetic field (see the blue shaded interval in Figure 2a). The peak magnetic field strength (|B|) of these structures reached approximately 13 nT, compared to a background magnetic field (B0) of about 4 nT, giving a ratio of |B|/B0 greater than 2.

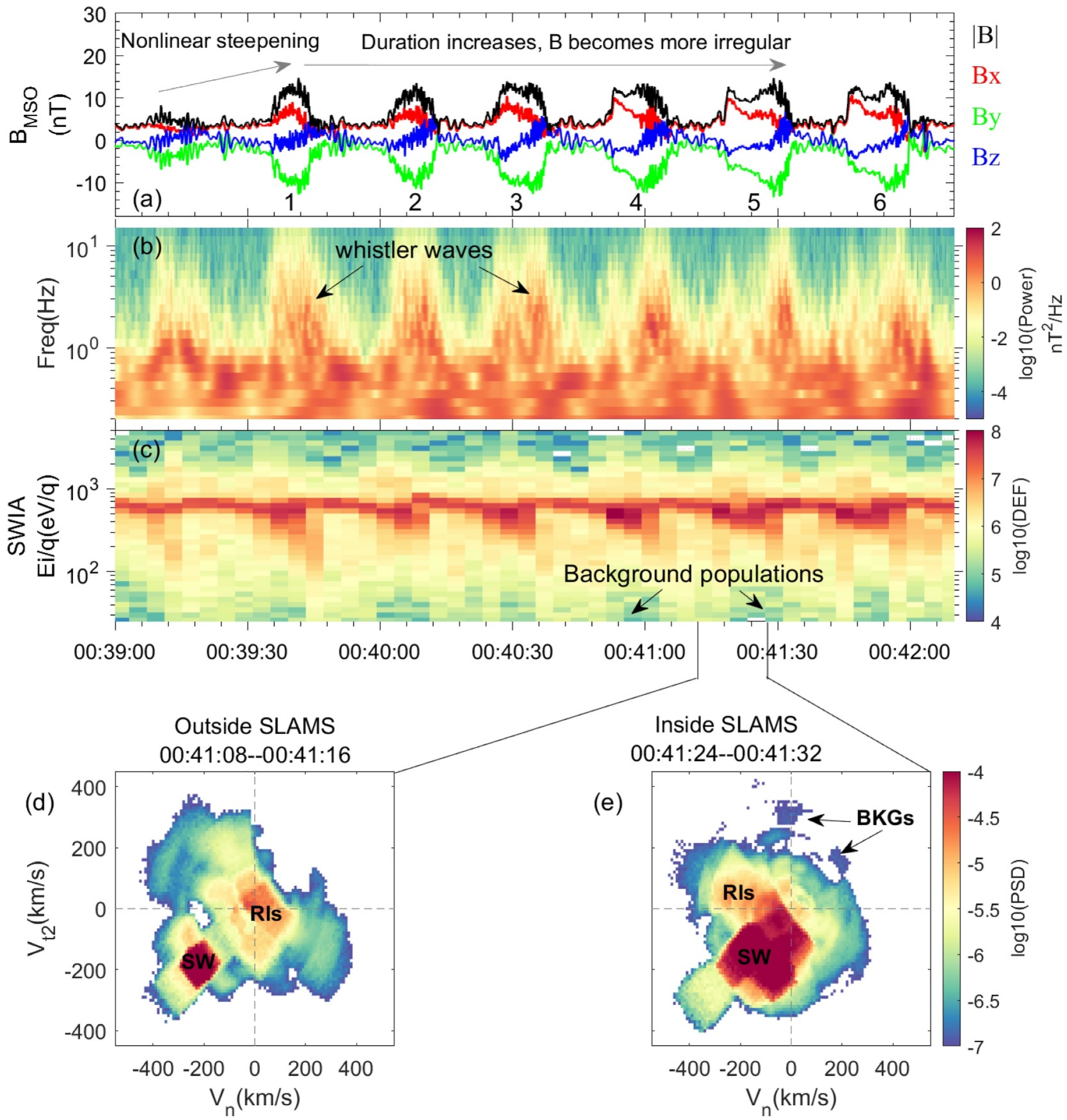


**Figure 3.** (a) Magnetic fields; (b) Magnetic field wave power spectrum; (c) Ion energy spectrum as measured by SWIA; (d, e) compare two-dimensional reduced ion distributions in the $\vec{n} - \vec{t}_2$ plane. The marker "SW" denotes the incident solar wind ions, "RIs" represents the reflected ions, and "BKGs" indicates the background populations.

These features are consistent with SLAMS (Chen et al., 2022; Lucek et al., 2008; Schwartz et al., 1992; Shuvalov & Grigorenko, 2023). From Figures 2a–2f, it is evident that the SLAMS exhibit the same magnetic field profiles and share the same periodicity with the upstream ULF waves, suggesting that these SLAMS originated from the nonlinear steepening of the ULF wave (Chen et al., 2021). These SLAMS are associated with broadband whistler waves, with frequencies ranging between 0.1 and 10 Hz (see Figures 2b; Wilson, 2016).

To illustrate the evolution of ULF waves and SLAMS as they approach the shock, Figure 3 provides detailed views of a ULF wave packet and six sequentially labeled SLAMS, numbered "1" through "6". Between 00:39:00 and 00:39:30, the ULF waves steepen nonlinearly, evolving into SLAMS "1" that exhibit a similar pattern of magnetic field variation (see Figure 3a). As we progress from SLAMS "1" to "5", the time duration of the SLAMS increases, the magnetic field becomes more irregular, and their boundaries become steeper. These features imply that the SLAMS progressively grow as they approach the bow shock.

The distribution of whistler waves varies across different stages of SLAMS evolution. In the early stages, specifically within SLAMS "1" and "2", whistler waves are observed at the center, similar to those in ULF waves (see

Figure 3b). However, for SLAMS "3" through "6", the whistler waves are predominantly observed at the trailing (upstream) edge, similar to whistler precursors (e.g., Y. Wang et al., 2023; M. Wang et al., 2024; S. Wang et al., 2024). This variation leads us to categorize SLAMS "1" and "2" as partially developed, and SLAMS "3" through "6" are fully developed.

We construct a coordinate system defined as $\{\vec{n}, \vec{t}_1, \vec{t}_2\}$, where $\vec{n}$ represents the shock normal vector pointing from the shock toward the upstream (see Table 1), $\vec{t}_1$ and $\vec{t}_2$ are tangent to the shock surface (Graham et al., 2024; Schwartz, 1998). The vector $\vec{t}_2$ can be estimated as $\vec{t}_2 = \vec{n} \times \vec{B}_{\text{up}} / |\vec{n} \times \vec{B}_{\text{up}}|$, which approximates to $(0.45, 0.41, -0.79)$. Figures 3d and 3e show the two-dimensional reduced velocity distributions of ions outside and inside the SLAMS, respectively. It is evident that the incident solar wind ions, referred to as "SW", is located in the lower left corner of the velocity distributions with negative $V_n$ components and high flux (referred to as "SW"). A comparison of these two distributions reveals that the "SW" exhibit a lower velocity and broader distribution inside the SLAMS, suggesting that it was decelerated and heated within the SLAMS. This also confirms that the upstream boundary of SLAMS represents a small-scale shock. By utilizing the mixed-mode coplanarity method, we determined that the normal direction of the upstream boundary of SLAM "5" is approximately (0.80, 0.15, 0.58), with a $\theta_{\text{Bn}}$ of about 53.68°. Similarly, for SLAM "6", the normal direction is approximately (0.78, 0.07, 0.62), with a $\theta_{\text{Bn}}$ of about 54.65°. These results closely align with the characteristics of the main shock (see Table 1).

In addition to "SW", there is a significant change in the behavior of reflected ions across the SLAMS, referred to as "RIs". Outside the SLAMS, the reflected ions have low velocities and primarily positive $V_n$ components, indicating movement toward the upstream region. However, inside the SLAMS, the reflected ions move toward the shock with negative $V_n$ components and positive $V_{t2}$ components. This can be attributed to the shock-reflected ions being reflected again by the shock-like boundary of the SLAMS, causing the reflected ions to move toward the shock (Wilson et al., 2013). This process closely resembles the behavior of ions reflected by the upstream shock-like boundary of foreshock transients (e.g., Turner et al., 2018; 2021). Moreover, we also observe a diffuse population in both the energy spectrum and velocity distributions (see Figures 3c–3e). This population may originate from instrumental background signals ("BKGs") or pickup protons. However, their impact on our analysis is negligible due to their significantly lower flux compared to that of the reflected and incident solar wind ions.

The evolution of ULF waves into SLAMS, coupled with their modulation of solar wind ions and reflected ions, and the similarity between the characteristics of the SLAMS and the main shock, strongly indicates the shock reformation process (e.g., Johlander et al., 2022). Additionally, the periodic magnetic field fluctuations observed in the downstream magnetosheath, which echo the patterns of the upstream ULF waves and SLAMS (see Figures 2e–2g), lend further support to the reformation scenario (Madanian et al., 2020). This finding is surprising, as such reformation processes typically occur in quasi-parallel shocks at other planets, yet we observe it happening in the oblique shock at Mars. At Earth, although ULF waves and SLAMS are occasionally observed in oblique or quasi-perpendicular shocks (Bergman et al., 2025; Wang et al., 2019, 2024), shock reformation driven by SLAMS steepening from ULF waves is unlikely to occur in such shock configurations.

Another notable aspect of the observed reformation is that the peak magnetic field magnitude within these SLAMS exceeds that of the main shock (see Figure 2a), suggesting that the newly formed shock, evolved from the SLAMS, can surpass the main shock. However, previous studies have shown that during shock reformation, the amplitude of SLAMS typically increases to become comparable with that of the main shock, yet does not exceed it (Lefebvre et al., 2009). Moreover, given that the amplitude of SLAMS is proportional to the $M_A$ (Bergman et al., 2025; Karlsson et al., 2024), and considering that the analyzed shock is an oblique shock with a relatively low $M_A$ compared to typical values, it is unlikely to produce such high-amplitude SLAMS. Therefore, the shock reformation on Mars exhibits distinctive characteristics not observed on other planets.

### 3.2. Modulation of Reflected Ions

In this section, we show that ULF waves also modulate the dynamics of reflected ions. Figures 4a and 4b display the one-dimensional reduced ion distributions along the $V_n$ and $V_{t2}$ in the upstream region. In the normal direction, we observe a beam-like structure with $V_n = -260$ km/s, representing the incident solar wind ions. In contrast, the reflected ions display periodic, hole-like structures in the spectrum (see the black dashed ovals in Figure 4a),

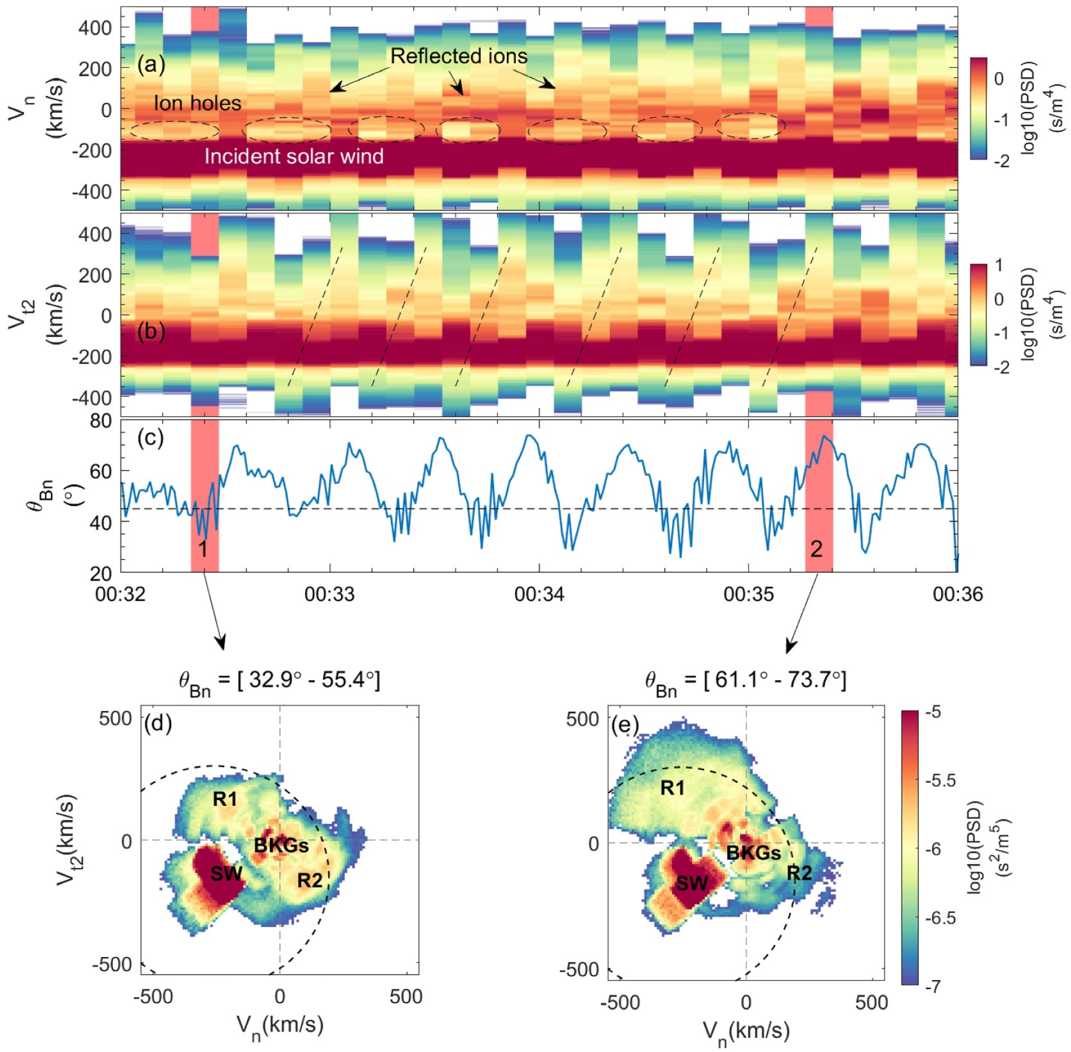


**Figure 4.** (a, b) Show the one-dimensional reduced ion distributions along $\vec{n}$ and $\vec{t}_2$, respectively. The dashed ovals in panel (a) represent the ion holes. (c) Shock normal angle. The dashed line represents the 45°. (d, e) show the two-dimensional reduced ion distributions in the $\vec{n} - \vec{t}_2$ plane. The black dashed circles indicate the theoretically predicted velocity distribution of specularly reflected ions based on $|\vec{V}_r - \vec{V}_u| = 2|V_{un}|$ (Graham et al., 2024; Khotyaintsev et al., 2024), where $\vec{V}_r$ represents the velocity of the specularly reflected ions, and $V_{un}$ is the normal speed of the incident solar wind ions. The marker "SW" denotes the incident solar wind ions, while markers "R1" and "R2" identify different populations of reflected ions. The marker "BKGs" represents the background populations. The time intervals for (d, e) correspond to intervals "1" and "2", respectively, as marked by the pink shaded regions in panels (a–c).

which are commonly referred to as ion holes (Yang et al., 2020). These periodic ion holes are typically observed during the shock reformation (e.g., Madanian et al., 2021). Additionally, the $V_{t2}$ components of reflected ions also show periodic variations, as indicated by the dashed line in Figure 4b.

Figure 4c shows the variation of $\theta_{\mathrm{Bn}}$ caused by the ULF waves. We can observe that $\theta_{\mathrm{Bn}}$ can decrease below 45° and increase above 70°, indicating that the bow shock periodically alternates among quasi-parallel, oblique, and quasi-perpendicular states. Figures 4a and 4b illustrate that during the quasi-parallel state with low $\theta_{\mathrm{Bn}}$, the reflected ions exhibit ion holes in the $V_n$ components, with most reflected ions having negative $V_{t2}$ components. Conversely, in the quasi-perpendicular state with high $\theta_{\mathrm{Bn}}$, most of the reflected ions display positive $V_{t2}$ components and negative $V_n$ components.

To further examine the response of the reflected ions to variations in $\theta_{\mathrm{Bn}}$, we selected two intervals with distinct $\theta_{\mathrm{Bn}}$ ranges, marked as "1" and "2" in Figure 4c. Interval "1" has $\theta_{\mathrm{Bn}}$ ranging from 32° to 55°, indicating a quasi-parallel and oblique state, while interval "2" spans from 61° to 74°, indicative of a quasi-perpendicular state. Figures 4d and 4e illustrate the 2-dimensional reduced velocity distributions of ions in interval "1" and interval "2", respectively. Regarding the reflected ions, we observe two distinct groups in both intervals. One group, marked as "R1", shows positive $V_{t2}$ and negative $V_n$ components, while the other group, marked as "R2", displays negative $V_{t2}$ and positive $V_n$ components. Compared with incident "SW", the R2 group exhibits similar, albeit slightly lower $V_{t2}$ values and opposite $V_n$ values. These ions align with specularly reflected ions, whose normal velocity is reversed while their tangential velocity remains largely unchanged upon reflection at the shock (Paschmann et al., 1982). Comparing Figures 4d and 4e, we observe that R2 shows no significant variation across different values of $\theta_{\mathrm{Bn}}$. This is expected, as specular reflection is largely dependent on $\vec{n}$, rather than on $\theta_{\mathrm{Bn}}$. Additionally, we observe a significant phase space density of background populations near $V_n \approx 0, V_{t2} \approx 0$.

After the reflection, these reflected ions are further accelerated by the solar wind motional electric field and begin to gyrate (e.g., Sckopke et al., 1983). During this process, the ion motion is strongly influenced by the $\theta_{\mathrm{Bn}}$ (Meziane et al., 2004; Schwartz et al., 1983). As they gyrate back toward the shock, their normal velocity $V_n$ gradually returns to negative values. Concurrently, the motional electric field accelerates the ions along the $\vec{t}_2$ direction, and the gyration motion cause their tangential velocity $V_{t2}$ to become positive and further increase. This eventually results in a population similar to that of group R1. Therefore, we interpret that the R1 is essentially the evolutionary result of R2. Further evidence for these ions being specularly reflected is that the observed velocity distributions of both R1 and R2 closely align with the theoretical prediction for specularly reflected ions, as represented by the black dashed circles in Figures 4d and 4e. Furthermore, by comparing Figures 4d and 4e, we observe that R1 exhibits a broader extension at higher values of $\theta_{\mathrm{Bn}}$. This behavior is clearly demonstrated by the simplified test-particle simulations, which reveal that $\theta_{\mathrm{Bn}}$ significantly influences the motion of reflected ions (refer to Figure S1 in the Supporting Information S1).

It should be noted that R1 could also represent ions reflected by the shock-like boundaries of SLAMS. However, the normal direction of these boundaries closely aligns with that of the main shock (see Section 3.1). Consequently, even if R1 ions are reflected by the SLAMS, their behavior is expected to closely mirror that of ions reflected by the main shock.

## 4. Conclusions and Discussions

In this study, we investigate the dynamics of shock reformation at Mars and reveal the role of upstream ULF waves on the bow shock dynamics. The key findings are summarized as follows:

1. Despite the oblique shock geometry ($\theta_{\mathrm{Bn}} = 51.6°$), we observe that ULF waves can nonlinearly steepen and evolve into SLAMS as they approach the shock. As these SLAMS move toward Mars, they grow further with the upstream boundary evolving into a small-scale shock. These SLAMS subsequently interacted with the shock, leading to the reformation of the shock. This is noteworthy as such type of reformation typically occurs in quasi-parallel shocks on other planets. Interestingly, the amplitude of the SLAMS exceeds that of the main shock during the shock reformation, which is unexpected. These results suggest that the shock dynamics at Mars exhibit characteristics distinct from those observed at other planets.
2. Although the shock configuration is oblique, the ULF waves can periodically modulate the shock normal angle. This modulation leads the shock to alternate among quasi-parallel, oblique, and quasi-perpendicular states. This periodic alternation further influences the motion of specularly reflected ions, mirroring behaviors observed at Earth's bow shock. Thus, the ULF wave increases the complexity of the bow shock plasma environments.

Our results indicate that Martian shock reformation differs from that observed at other planets. Previous studies showed that shock reformation strongly depends on its geometric configuration. SLAMS or other nonlinearly steepened waves (e.g., Shocklets) are responsible for the reformation of quasi-parallel shocks (Johlander et al., 2022; Raptis et al., 2022). In contrast, the self-reformation of quasi-perpendicular shocks is driven by the periodic formation of new ramps (Mazelle & Lembège, 2021; Yang et al., 2020). Here we observe reformation signatures of oblique shock similar to those occurred in quasi-parallel shocks. Additionally, we have identified two more cases of quasi-perpendicular shocks that closely parallel our observed oblique shock case (see Figure 5). In each case, as illustrated in Figures 5a1–5a2, the upstream ULF waves steepen and evolve into nonlinear structures as they approach the shock, indicative of shock reformation. Moreover, these ULF waves, as illustrated in Figures 5b1–5b2, occur at the frequency of the local proton gyrofrequency and propagate parallel to the

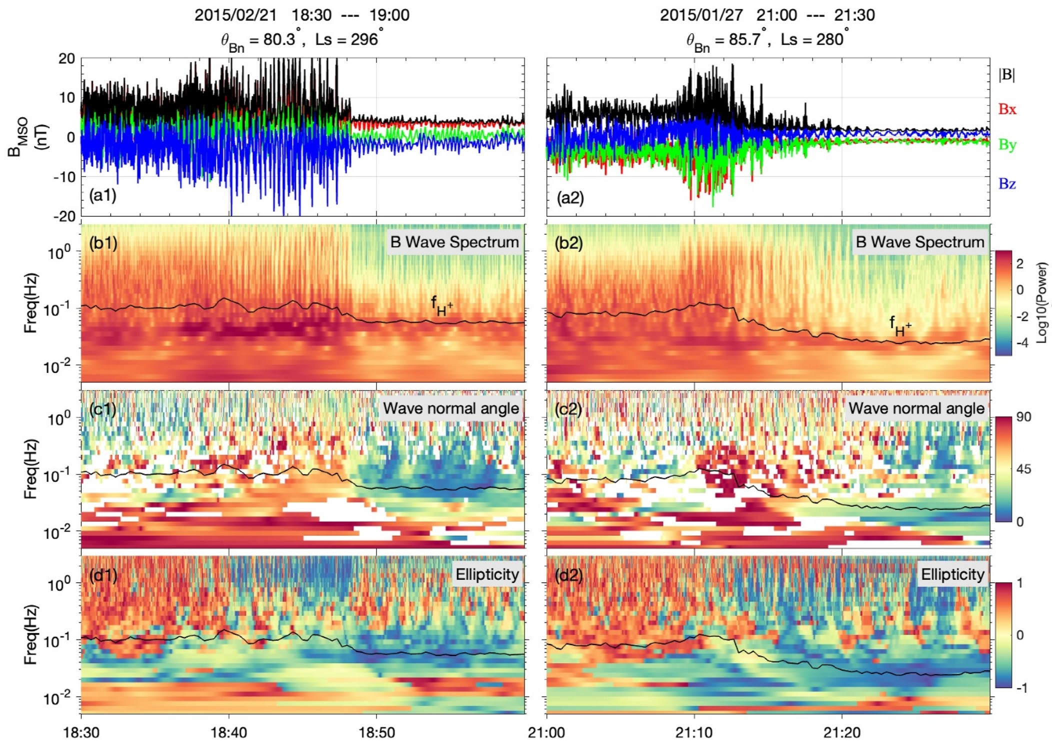


**Figure 5.** Two cases of quasi-perpendicular shock ($\theta_{\mathrm{Bn}} > 70°$) reformation driven by ultra-low frequency waves near perihelion (Ls ~ 270°). The left and right panels depict cases from 21 February 2015 and 27 January 2015, respectively. Panels (a1–a2) display magnetic field measurements. Panels (b1–b2) illustrate the magnetic field power spectrum. Panels (c1–c2) show the wave normal angle. Panels (d1–d2) present the ellipticity of the waves.

ambient magnetic field, as shown in Figures 5c1–5c2. They also exhibit left-handed polarization in the spacecraft frame, as observed in Figures 5d1–5d2. These characteristics are consistent with those observed in the analyzed oblique shock case depicted in Figure 2. Thus, we propose that a common physical mechanism underlies all these cases. We also note that the magnetic field signatures of the periodic formation of the quasi-perpendicular shock reported by Shan et al. (2020) are also similar to those observed in our case. Thus, it appears that this type of shock reformation is less dependent on shock geometry at Mars compared to other planets.

Why is shock reformation at Mars unique? This can be attributed to the distinct source of ULF waves at Mars. At other planets, the upstream ULF waves are primarily foreshock ULF waves, which are generated by reflected ions and confined to the quasi-parallel regions. Thus, the shock reformation driven by the nonlinear steepening of ULF waves, observed exclusively in quasi-parallel shocks of other planets. However, at Mars, the planetary ions can be generated in the upstream region regardless of the shock geometry, which leads to the production of PCWs over a broader spatial range. These PCWs may also evolve into SLAMS and trigger the shock reformation. Consequently, such type of shock reformation can be observed across various shock geometries at Mars. This is expected to be particularly pronounced near perihelion (Ls ~ 270°), due to the high intensity and occurrence rate of PCWs (Bertucci et al., 2013; Romanelli et al., 2016; Romeo et al., 2021; Yamauchi, Lundin et al., 2015; Yamauchi, Hara et al., 2015). Interestingly, the oblique shock case presented in Figure 1 and the quasi-perpendicular cases shown in Figure 5 all occurred near the perihelion, aligning with our expectation. Therefore, we propose that on Mars, the presence of planetary ions may not only create a planetary ion foreshock as reported by Yamauchi, Lundin et al. (2015), Yamauchi, Hara et al. (2015), but also introduce additional ULF waves and further affect the shock dynamics.

This could also explain why the ULF waves and SLAMS exhibit such large amplitudes in the shock reformation. In other planetary shocks, the free energy for ULF waves and SLAMS primarily stems from the shock itself (ions reflected by the shock), thus the amplitude of these waves and SLAMS is controlled by the $M_A$ and $\theta_{\mathrm{Bn}}$. During shock reformation, although SLAMS tend to grow as they approach the main shock, their amplitudes do not exceed

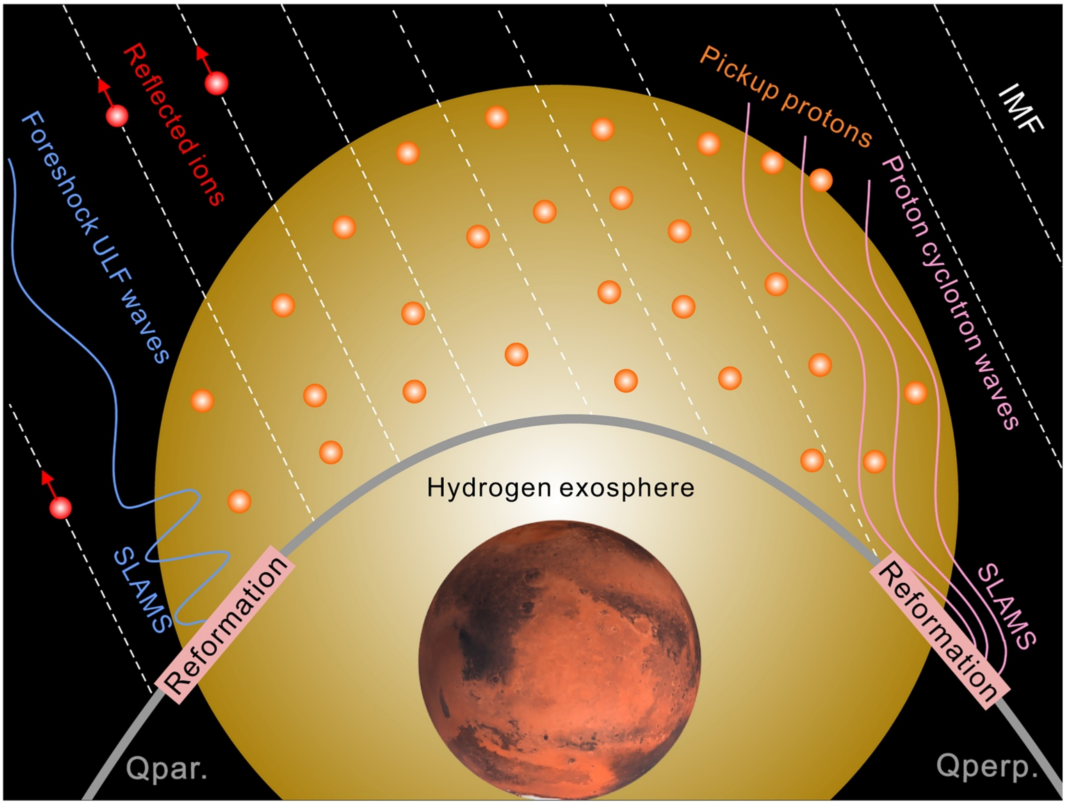


**Figure 6.** Schematic of shock reformation driven by ultra-low frequency (ULF) waves at Mars. On the left side, which is the quasi-parallel shock side (marked as "Qpar."), the reflected ions (red circles with arrows) can travel along the IMF to the upstream region, initiating the foreshock ULF waves (blue curve). These foreshock ULF waves may steepen as they move toward the shock, evolve into short large-amplitude magnetic structures (SLAMS), and subsequently drive shock reformation. The neutral hydrogen exosphere (dark yellow circles) can extend beyond the bow shock. Once the neutral particles are ionized, they become pickup ions (light yellow circles) that interact with the solar wind, generating proton cyclotron waves (PCWs) (pink curve). On the right side, which is the quasi-perpendicular shock side (marked as "Qperp."), the PCWs can evolve into SLAMS as they move toward the shock, also leading to shock reformation.

that of the main shock itself (Lefebvre et al., 2009). In our case, however, the free energy generating the ULF waves and SLAMS originates from additional sources (planetary ions). This could allow their amplitudes to exceed that of the main shock during reformation. This indicates that planetary ions play a significant role in the shock dynamics at Mars, making the Martian bow shock an exceptionally valuable laboratory for studying shocks and the associated fundamental plasma physics. In addition to the influence of planetary ions, it is important to note that, compared to the magnetosheath, the ions within SLAMS are not fully thermalized. This partial thermalization may also contribute to the enhanced amplitude of SLAMS (Schwartz et al., 1992). Therefore, the unexpectedly high amplitude of SLAMS may result from a combination of factors. It is important to note that our results do not suggest this type of reformation is entirely independent of shock geometry. In quasi-parallel shock regions, reflected ions have more time and space to interact with the incoming solar wind, resulting in a higher occurrence rate of ULF waves. Therefore, this reformation process remains more prominent on the quasi-parallel side.

In addition to affecting the upstream region and the shock, the ULF waves also influence the dynamics of the magnetosheath. The magnetosheath jets has recently been observed at Mars (Gunnel et al., 2023; Mohammed-Amin et al., 2025). The formation of these jets may be linked to SLAMs and the shock reformation process (Kramer et al., 2025, Section 2.2), both of which are related to ULF waves. Consequently, our findings imply that jet formation related to upstream ULF waves could be significant not only in the quasi-parallel magnetosheath but might also extend to the quasi-perpendicular magnetosheath at Mars.

In summary, we propose that shock reformation driven by ULF waves at Mars can occur across all shock geometries, as illustrated in Figure 6. On the quasi-parallel side, foreshock ULF waves, triggered by reflected ions,

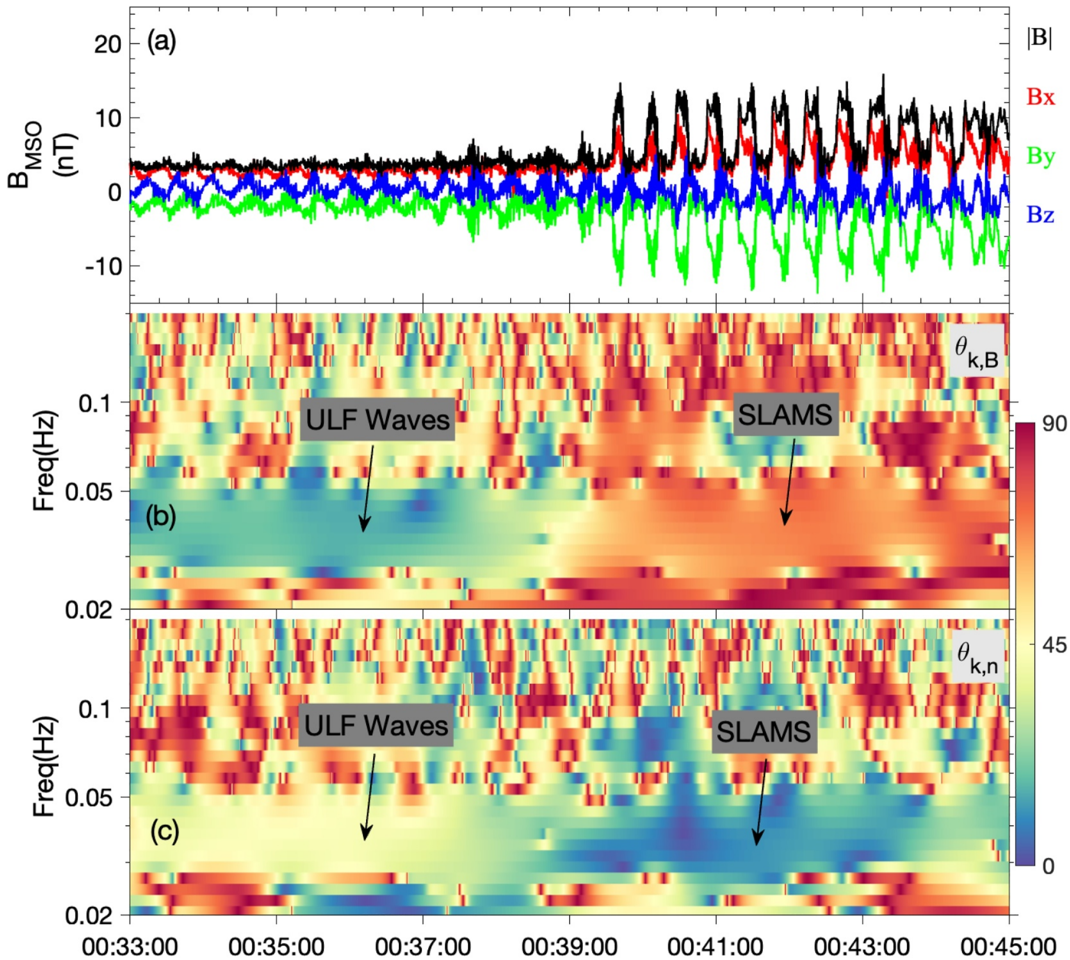


**Figure 7.** (a) Magnetic fields. (b) Wave normal angle (the angle between the wave vector and the background magnetic fields). (c) The angle between the wave vector and the normal direction of shock.

can steepen and evolve into SLAMS, subsequently driving shock reformation. On the quasi-perpendicular side, pickup protons can trigger the formation of PCWs. Similar to foreshock ULF waves, these PCWs can evolve into SLAMS as they approach the shock, then similarly drive shock reformation. However, the evolution from PCWs to SLAMS and the subsequent shock reformation may differ from those observed in quasi-parallel shocks which are driven by the foreshock ULF waves, which remain unclear and require further numerical simulations for comprehensive elucidation.

Interestingly, recent research by Xu et al. (2025) proposed that whistler waves can drive the reformation of quasi-perpendicular shocks. Their simulations show that the wave vector of whistler waves is initially aligned with the upstream background magnetic field and nearly perpendicular to the shock normal, but becomes aligned with the shock normal as the waves approach the shock. Our observations reveal a similar pattern: the ULF waves propagate along the background magnetic field lines (see Figures 7a and 7b) and are nearly perpendicular to the shock normal (see Figure 7c). As the shock is approached, the wave vector of the SLAMS becomes nearly parallel to the shock normal and perpendicular to the background magnetic field. These parallels suggest that the shock reformation process driven by PCWs may operate through a mechanism analogous to that of whistler waves, despite differences in wave mode.

## Conflict of Interest

The authors declare no conflicts of interest relevant to this study.

## Data Availability Statement

The research described in this manuscript utilizes publicly available data from the MAVEN mission, including data from the SWIA, SWEA, MAG, and STATIC instruments (Connerney, 2023; Halekas, 2017; McFadden, 2023; Mitchell, 2023). The data analysis was performed using the irfu-matlab software package (Khotyaintsev et al., 2022).

**Acknowledgments**
This work was partially supported by NASA Grant NNH10CC04C through the MAVEN Project, NASA Grants 80NSSC23K0911 and 80NSSC24K1843, and the Alfred P. Sloan Research Fellowship. SR acknowledges support from the Johns Hopkins University Applied Physics Laboratory independent R&D fund. Parts of this work for the observations obtained with the SWEA instrument are supported by the French space agency CNES (National Centre for Space Studies). We acknowledge fruitful discussions with James P. McFadden.

## References

Andrés, N., Romanelli, N., Mazelle, C., Chen, L. J., Gruesbeck, J. R., & Espley, J. R. (2025). Foreshock ultralow frequency waves at Mars: Consequence on the particle acceleration mechanisms at the Martian bow shock. *The Astrophysical Journal*, *979*(1), 77. https://doi.org/10.3847/1538-4357/ada250

Balikhin, M., & Gedalin, M. (2022). Collisionless shocks in the heliosphere: Foot width revisited. *The Astrophysical Journal*, *925*(1), 90. https://doi.org/10.3847/1538-4357/ac3bb3

Barabash, S., & Lundin, R. (1993). Reflected ions on Mars: Phobs-2 observations. *Geophysical Research Letters*, *20*(9), 787–790. https://doi.org/10.1029/93GL00834

Bergman, S., Karlsson, T., Wong Chan, T. K., & Trollvik, H. (2025). Statistical properties of Short Large-Amplitude Magnetic Structures (SLAMS) in the foreshock of Earth from cluster measurements. *Journal of Geophysical Research: Space Physics*, *130*(3). https://doi.org/10.1029/2024ja033568

Bertucci, C., Romanelli, N., Chaufray, J. Y., Gomez, D., Mazelle, C., Delva, M., et al. (2013). Temporal variability of waves at the proton cyclotron frequency upstream from Mars: Implication for Mars distant hydrogen exosphere. *Geophysical Research Letters*, *40*(15), 3809–3813. https://doi.org/10.1002/grl.50709

Burgess, D., Möbius, E., & Scholer, M. (2012). Ion acceleration at the Earth's bow shock. *Space Science Reviews*, *173*(1–4), 5–47. https://doi.org/10.1007/s11214-012-9901-5

Burgess, D., & Scholer, M. (2015). *Collisionless shocks in space plasmas: Structure and accelerated particles*. Cambridge University Press.

Burne, S., Bertucci, C., Mazelle, C., Morales, L. F., Meziane, K., Halekas, J., et al. (2021). The structure of the Martian quasi-perpendicular supercritical shock as seen by MAVEN. *Journal of Geophysical Research: Space Physics*, *126*(9). https://doi.org/10.1029/2020ja028938

Chaffin, M. S., Chaufray, J. Y., Deighan, J., Schneider, N. M., McClintock, W. E., Stewart, A. I. F., et al. (2015). Three-dimensional structure in the Mars H corona revealed by IUVS on MAVEN. *Geophysical Research Letters*, *42*(21), 9001–9008. https://doi.org/10.1002/2015gl065287

Chen, L. J., Halekas, J., Wang, S., DiBraccio, G. A., Romanelli, N., et al. (2022). Solitary magnetic structures developed from gyro-resonance with solar wind ions at Mars and Earth. *Geophysical Research Letters*, *49*(3). https://doi.org/10.1029/2021gl097600

Chen, L. J., Wang, S., Ng, J., Bessho, N., Tang, J., Fung, S. F., et al. (2021). Solitary magnetic structures at quasi-parallel collisionless shocks: Formation. *Geophysical Research Letters*, *48*(1), e2021GL093029. https://doi.org/10.1029/2020gl090800

Collinson, G. A., Hietala, H., Plaschke, F., Karlsson, T., Wilson, L. B., III, Archer, M., et al. (2023). Shocklets and Short Large Amplitude Magnetic Structures (SLAMS) in the high Mach foreshock of Venus. *Geophysical Research Letters*, *50*(18). https://doi.org/10.1029/2023gl104610

Connerney, J., Espley, J., Lawton, P., Murphy, S., Odom, J., Oliversen, R., & Sheppard, D. (2015). The MAVEN magnetic field investigation. *Space Science Reviews*, *195*(1–4), 257–291. https://doi.org/10.1007/s11214-015-0169-4

Connerney, J. E. P. (2023). MAVEN Magnetometer (MAG) calibrated data bundle [Dataset]. *NASA Planetary Data System*. https://doi.org/10.17189/1414178

Delva, M., Mazelle, C., & Bertucci, C. (2011). Upstream Ion Cyclotron Waves at Venus and Mars. *Space Science Reviews*, *162*(1–4), 5–24. https://doi.org/10.1007/s11214-011-9828-2

Eastwood, J. P., Balogh, A., Lucek, E. A., Mazelle, C., & Dandouras, I. (2005). Quasi-monochromatic ULF foreshock waves as observed by the four-spacecraft cluster mission: 1. Statistical properties. *Journal of Geophysical Research*, *110*(A11). https://doi.org/10.1029/2004ja010617

Eastwood, J. P., Lucek, E. A., Mazelle, C., Meziane, K., Narita, Y., Pickett, J., & Treumann, R. A. (2005). The foreshock. *Space Science Reviews*, *118*(1–4), 41–94. https://doi.org/10.1007/s11214-005-3824-3

Fruchtman, J., Halekas, J., Gruesbeck, J., Mitchell, D., & Mazelle, C. (2023). Seasonal and Mach number variation of the Martian bow shock structure. *Journal of Geophysical Research: Space Physics*, *128*(8). https://doi.org/10.1029/2023ja031759

Gary, S. P. (1991). Electromagnetic ion/ion instabilities and their consequences in space plasmas: A review. *Space Science Reviews*, *56*(3–4). https://doi.org/10.1007/bf00196632

Gosling, J. T., Thomsen, M. F., Bame, S. J., Feldman, P. D., Paschmann, G., & Sckopke, N. (1982). Evidence for specularly reflected ions upstream from quasi-parallel shock. *Geophysical Research Letters*, *9*(12), 1333–1336. https://doi.org/10.1029/GL009i012p01333

Graham, D. B., Khotyaintsev, Y. V., Dimmock, A. P., Lalti, A., Boldú, J. J., Tigik, S. F., & Fuselier, S. A. (2024). Ion dynamics across a low Mach number bow shock. *Journal of Geophysical Research: Space Physics*, *129*(4). https://doi.org/10.1029/2023ja032296

Gruesbeck, J. R., Espley, J. R., Connerney, J. E. P., DiBraccio, G. A., Soobiah, Y. I., Brain, D., et al. (2018). The three-dimensional bow shock of Mars as observed by MAVEN. *Journal of Geophysical Research: Space Physics*, *123*(6), 4542–4555. https://doi.org/10.1029/2018ja025366

Gunell, H., Hamrin, M., Nesbit-Östman, S., Krämer, E., & Nilsson, H. (2023). Magnetosheath jets at Mars. *Science Advances*, *9*(22), eadg5703. https://doi.org/10.1126/sciadv.adg5703

Halekas, J. S. (2017). MAVEN Solar Wind Ion Analyzer (SWIA) calibrated data bundle [Dataset]. *NASA Planetary Data System*. https://doi.org/10.17189/1414182

Halekas, J. S., Shaver, S., Azari, A. R., Fowler, C. M., Ma, Y., Xu, S., et al. (2023). The day the solar wind disappeared at Mars. *Journal of Geophysical Research: Space Physics*, *128*(12), e2023JA031935. https://doi.org/10.1029/2023JA031935

Halekas, J. S., Taylor, E. R., Dalton, G., Johnson, G., Curtis, D. W., McFadden, J. P., et al. (2015). The solar wind ion analyzer for MAVEN. *Space Science Reviews*, *195*(1–4), 125–151. https://doi.org/10.1007/s11214-013-0029-z

Jakosky, B. M., Lin, R. P., Grebowsky, J. M., Luhmann, J. G., Mitchell, D. F., Beutelschies, G., et al. (2015). The Mars Atmosphere and Volatile EVOLUTION (MAVEN) Mission. *Space Science Reviews*, *195*(1–4), 3–48. https://doi.org/10.1007/s11214-015-0139-x

Johlander, A., Battarbee, M., Turc, L., Ganse, U., Pfau-Kempf, Y., Grandin, M., et al. (2022). Quasi-parallel shock reformation seen by magnetospheric multiscale and ion-kinetic simulations. *Geophysical Research Letters*, *49*(2), e2021GL096335. https://doi.org/10.1029/2021GL096335

Kajdič, P., Pfau-Kempf, Y., Turc, L., Dimmock, A. P., Palmroth, M., Takahashi, K., et al. (2021). ULF wave transmission across collisionless shocks: 2.5D local hybrid simulations. *Journal of Geophysical Research: Space Physics*, *126*(11). https://doi.org/10.1029/2021ja029283

Karlsson, T., Plaschke, F., Glass, A. N., & Raines, J. M. (2024). Short Large-Amplitude Magnetic Structures (SLAMS) at mercury observed by MESSENGER. *Annales Geophysicae*, *42*(1), 117–130. https://doi.org/10.5194/angeo-42-117-2024

Khotyaintsev, Y., et al. (2022). irfu/irfu-matlab: V1.16.3 (v1.16.3) [Software]. *Zenodo*. https://doi.org/10.5281/zenodo.11550091

Khotyaintsev, Y. V., Graham, D. B., & Johlander, A. (2024). Ion reflection by a rippled perpendicular shock. *Physical Review Letters*, *133*(21), 215201. https://doi.org/10.1103/PhysRevLett.133.215201

Krämer, E., Koller, F., Suni, J., LaMoury, A. T., Pöppelwerth, A., Glebe, G., et al. (2025). Jets downstream of collisionless shocks: Recent discoveries and challenges. *Space Science Reviews*, *221*(1), 4. https://doi.org/10.1007/s11214-024-01129-3

Lefebvre, B., Seki, Y., Schwartz, S. J., Mazelle, C., & Lucek, E. A. (2009). Reformation of an oblique shock observed by cluster. *Journal of Geophysical Research*, *114*(A11), A11107. https://doi.org/10.1029/2009JA014268

Li, J. H., Zhou, X., Wang, S., Liu, Z., Zong, Q., Yao, S., et al. (2024). Bow shock ripples and their modulation of whistler wave packets: MMS observations. *Geophysical Research Letters*, *51*(20). https://doi.org/10.1029/2024gl111590

Liu, D., Yao, Z., Wei, Y., Rong, Z., Shan, L., Arnaud, S., et al. (2020). Upstream proton cyclotron waves: Occurrence and amplitude dependence on IMF cone angle at Mars—From MAVEN observations. *Earth and Planetary Physics*, *4*(1), 1–11. https://doi.org/10.26464/epp2020002

Liu, T., Angelopoulos, V., & Lu, S. (2019). Relativistic electrons generated at Earth's quasi-parallel bow shock. *Science Advances*, *5*(7), eaaw1368. https://doi.org/10.1126/sciadv.aaw1368

Liu, T. Z., Hao, Y., Wilson, L. B., Turner, D. L., & Zhang, H. (2021). Magnetospheric multiscale observations of Earth's oblique bow shock reformation by foreshock ultralow-frequency waves. *Geophysical Research Letters*, *48*(2). https://doi.org/10.1029/2020gl091184

Lucek, E. A., Horbury, T. S., Dandouras, I., & Rème, H. (2008). Cluster observations of the Earth's quasi-parallel bow shock. *Journal of Geophysical Research*, *113*(A7). https://doi.org/10.1029/2007ja012756

Madanian, H., Desai, M. I., Schwartz, S. J., Wilson, L. B., III, Fuselier, S. A., Burch, J. L., et al. (2021). The dynamics of a high Mach number quasi-perpendicular shock: MMS observations. *The Astrophysical Journal*, *908*(1), 40. https://doi.org/10.3847/1538-4357/abcb88

Madanian, H., Omidi, N., Sibeck, D. G., Andersson, L., Ramstad, R., Xu, S., et al. (2023). Transient foreshock structures upstream of Mars: Implications of the small Martian bow shock. *Geophysical Research Letters*, *50*(8). https://doi.org/10.1029/2022gl101734

Madanian, H., Schwartz, S. J., Halekas, J. S., & Wilson, L. B. (2020). Nonstationary quasiperpendicular shock and ion reflection at Mars. *Geophysical Research Letters*, *47*(11). https://doi.org/10.1029/2020gl088309

Masunaga, K., Seki, K., Brain, D. A., Fang, X., Dong, Y., Jakosky, B. M., et al. (2016). $O^+$ ion beams reflected below the Martian bow shock: MAVEN observations. *Journal of Geophysical Research: Space Physics*, *121*(4), 3093–3107. https://doi.org/10.1002/2016ja022465

Mazelle, C., & Lembège, B. (2021). Evidence of the nonstationarity of the terrestrial bow shock from multi-spacecraft observations: Methodology, results, and quantitative comparison with Particle-In-Cell (PIC) simulations. *Annales Geophysicae*, *39*(4), 571–598. https://doi.org/10.5194/angeo-39-571-2021

Mazelle, C., Winterhalter, D., Sauer, K., Trotignon, J. G., Acuna, M., Baumgärtel, K., et al. (2004). Bow shock and upstream phenomena at Mars. *Space Science Reviews*, *111*(1/2), 115–181. https://doi.org/10.1023/B:SPAC.0000032717.98679.d0

McFadden, J., Kortmann, O., Curtis, D., Dalton, G., Johnson, G., Abiad, R., et al. (2015). MAVEN Suprathermal and Thermal Ion Composition (STATIC) instrument. *Space Science Reviews*, *195*(1–4), 199–256. https://doi.org/10.1007/s11214-015-0175-6

McFadden, J. P. (2023). MAVEN Suprathermal and Thermal Ion Composition (STATIC) calibrated data bundle [Dataset]. *NASA Planetary Data System*. https://doi.org/10.17189/1517741

Meziane, K., Mazelle, C., Wilber, M., LeQuéau, D., Eastwood, J. P., Rème, H., et al. (2004). Bow shock specularly reflected ions in the presence of low-frequency electromagnetic waves: A case study. *Annales Geophysicae*, *22*(7), 2325–2335. https://doi.org/10.5194/angeo-22-2325-2004

Mitchell, D. L. (2023). MAVEN Solar Wind Electron Analyzer (SWEA) calibrated data bundle [Dataset]. *NASA Planetary Data System*. https://doi.org/10.17189/1414181

Mitchell, D. L., Mazelle, C., Sauvaud, J. A., Thocaven, J. J., Rouzaud, J., Fedorov, A., et al. (2016). The MAVEN solar wind electron analyzer. *Space Science Reviews*, *200*(1–4), 495–528. https://doi.org/10.1007/s11214-015-0232-1

Mohammed-Amin, T., Krämer, E., Nesbit-Östman, S., Gunell, H., & Simon Wedlund, C. (2025). Jets downstream of the Martian bow shock. *Astronomy and Astrophysics*, *696*, A75. https://doi.org/10.1051/0004-6361/202453557

Paschmann, G., Sckopke, N., Bame, S. J., & Gosling, J. T. (1982). Observation of gyrating ions in the foot of the perpendicular shock. *Geophysical Research Letters*, *9*. https://doi.org/10.1029/GL009i008p00881

Raptis, S., Karlsson, T., Vaivads, A., Pollock, C., Plaschke, F., Johlander, A., et al. (2022). Downstream high-speed plasma jet generation as a direct consequence of shock reformation. *Nature Communications*, *13*(1), 598. https://doi.org/10.1038/s41467-022-28110-4

Richer, E., Chanteur, G. M., Modolo, R., & Dubinin, E. (2012). Reflection of solar wind protons on the Martian bow shock: Investigations by means of 3-dimensional simulations. *Geophysical Research Letters*, *39*(17). https://doi.org/10.1029/2012gl052858

Romanelli, N., Mazelle, C., Chaufray, J. Y., Meziane, K., Shan, L., Ruhunusiri, S., et al. (2016). Proton cyclotron waves occurrence rate upstream from Mars observed by MAVEN: Associated variability of the Martian upper atmosphere. *Journal of Geophysical Research: Space Physics*, *121*(11), 113–128. https://doi.org/10.1002/2016ja023270

Romanelli, N., Mazelle, C., & Meziane, K. (2018). Nonlinear wave-particle interaction: Implications for newborn planetary and backstreaming proton velocity distribution functions. *Journal of Geophysical Research: Space Physics*, *123*(2), 1100–1117. https://doi.org/10.1002/2017ja024691

Romeo, O. M., Romanelli, N., Espley, J. R., Mazelle, C., DiBraccio, G. A., Gruesbeck, J. R., & Halekas, J. S. (2021). Variability of Upstream proton cyclotron wave properties and occurrence at Mars observed by MAVEN. *Journal of Geophysical Research: Space Physics*, *126*(2). https://doi.org/10.1029/2020ja028616

Ruhunusiri, S., Halekas, J. S., Espley, J. R., Eparvier, F., Brain, D., Mazelle, C., et al. (2018). One-hertz waves at Mars: MAVEN observations. *Journal of Geophysical Research: Space Physics*, *123*(5), 3460–3476. https://doi.org/10.1029/2017ja024618

Schwartz, S. J. (1998). Shock and discontinuity normal, Mach numbers, and related parameters. In G. Paschmann & P. W. Daly (Eds.), *Analysis methods for multi-spacecraft data* (pp. 249–270).

Schwartz, S. J., Burgess, D., Wilkinson, W. P., Kessel, R. L., Dunlop, M., & Lühr, H. (1992). Observations of short large-amplitude magnetic structures at a quasi-parallel shock. *Journal of Geophysical Research*, *97*(A4), 4209–4227. https://doi.org/10.1029/91ja02581

Schwartz, S. J., Thomsen, M. F., & Gosling, J. T. (1983). Ions upstream of the Earth's bow shock: A theoretical comparison of alternative source populations. *Journal of Geophysical Research*, *88*(A3), 2039–2047. https://doi.org/10.1029/JA088iA03p02039

Sckopke, N., Paschmann, G., Bame, S. J., Gosling, J. T., & Russell, C. T. (1983). Evolution of ion distributions across the nearly perpendicular bow shock: Specularly and non-specularly reflected-gyrating ions. *Journal of Geophysical Research*, *88*(A8), 6121–6136. https://doi.org/10.1029/JA088iA08p06121

Shan, L., Du, A., Tsurutani, B. T., Ge, Y. S., Lu, Q., Mazelle, C., et al. (2020). In situ observations of the formation of periodic collisionless plasma shocks from fast mode waves. *The Astrophysical Journal Letters*, *888*(2), L17. https://doi.org/10.3847/2041-8213/ab5db3

Shuvalov, S. D., & Grigorenko, E. E. (2023). Observation of SLAMS-Like structures close to Martian aphelion by MAVEN. *Journal of Geophysical Research: Space Physics*, *128*(5). https://doi.org/10.1029/2022ja031018

Sulaiman, A. H., Masters, A., Dougherty, M. K., Burgess, D., Fujimoto, M., & Hospodarsky, G. B. (2015). Quasiperpendicular high Mach number shocks. *Physical Review Letters*, *115*(12), 125001. https://doi.org/10.1103/PhysRevLett.115.125001

Sundberg, T., Boardsen, S. A., Slavin, J. A., Uritsky, V. M., Anderson, B. J., Korth, H., et al. (2013). Cyclic reformation of a quasi-parallel bow shock at Mercury: MESSENGER observations. *Journal of Geophysical Research: Space Physics*, *118*(10), 6457–6464. https://doi.org/10.1002/jgra.50602

Trotignon, J. G., Mazelle, C., Bertucci, C., & Acuña, M. H. (2006). Martian shock and magnetic pile-up boundary positions and shapes determined from the Phobos 2 and Mars global surveyor data sets. *Planetary and Space Science*, *54*(4), 357–369. https://doi.org/10.1016/j.pss.2006.01.003

Turner, D. L., Wilson, L. B., Goodrich, K. A., Madanian, H., Schwartz, S. J., Liu, T. Z., et al. (2021). Direct multipoint observations capturing the reformation of a supercritical fast magnetosonic shock. *The Astrophysical Journal Letters*, *911*(2), L31. https://doi.org/10.3847/2041-8213/abec78

Turner, D. L., Wilson, L. B., III, Liu, T. Z., Cohen, I. J., Schwartz, S. J., Osmane, A., et al. (2018). Autogenous and efficient acceleration of energetic ions upstream of Earth's bow shock. *Nature*, *561*(7722), 206–210. https://doi.org/10.1038/s41586-018-0472-9

Wang, M., Liu, T. Z., Zhang, H., Liu, K., Shi, Q., Guo, R., et al. (2024). Statistical analysis of whistler precursors upstream of foreshock transient shocks: MMS observations. *Geophysical Research Letters*, *51*(8). https://doi.org/10.1029/2023gl105617

Wang, S., Chen, L. J., Bessho, N., Hesse, M., Wilson, L. B., Giles, B., et al. (2019). Observational evidence of magnetic reconnection in the terrestrial bow shock transition region. *Geophysical Research Letters*, *46*(2), 562–570. https://doi.org/10.1029/2018gl080944

Wang, S., Li, J. H., Li, L., Zhou, X. Z., Omura, Y., Zhao, J. T., et al. (2024). A statistical examination of interactions between 1-Hz whistler waves and ions in the Earth's foreshock. *Journal of Geophysical Research: Space Physics*, *129*(10). https://doi.org/10.1029/2024ja032960

Wang, Y., Zhong, J., Slavin, J., Zhang, H., Lee, L. C., Shan, L., et al. (2023). MESSENGER observations of standing whistler waves upstream of mercury's bow shock. *Geophysical Research Letters*, *50*(10). https://doi.org/10.1029/2022gl102574

Wilson, L. B., Koval, A., Sibeck, D. G., Szabo, A., Cattell, C. A., Kasper, J. C., et al. (2013). Shocklets, SLAMS, and field-aligned ion beams in the terrestrial foreshock. *Journal of Geophysical Research: Space Physics*, *118*(3), 957–966. https://doi.org/10.1029/2012ja018186

Wilson III, L. B. (2016). Low frequency waves at and upstream of collisionless shocks. In A. Keiling, D.-H. Lee, & V. Nakariakov (Eds.), *Low-frequency waves in space plasmas, geophysical monograph series* (Vol. 216, pp. 269–291). AGU. https://doi.org/10.1002/9781119055006.ch16

Xu, S., Sun, J.-J., Wang, S., Li, J.-H., Zhou, X.-Z., Graham, D. B., et al. (2025). Shock reformation induced by ion-scale whistler waves in quasi-perpendicular bow shock. *Research Square*. https://doi.org/10.21203/rs.3.rs-6012766/v1

Yamauchi, M., Futaana, Y., Fedorov, A., Frahm, R. A., Dubinin, E., Lundin, R., et al. (2012). Ion acceleration by multiple reflections at Martian bow shock. *Earth Planets and Space*, *64*(2), 61–71. https://doi.org/10.5047/eps.2011.07.007

Yamauchi, M., Futaana, Y., Fedorov, A., Frahm, R. A., Winningham, J. D., Dubinin, E., et al. (2011). Comparison of accelerated ion populations observed upstream of the bow shocks at Venus and Mars. *Annales Geophysicae*, *29*(3), 511–528. https://doi.org/10.5194/angeo-29-511-2011

Yamauchi, M., Hara, T., Lundin, R., Dubinin, E., Fedorov, A., Sauvaud, J. A., et al. (2015). Seasonal variation of Martian pick-up ions: Evidence of breathing exosphere. *Planetary and Space Science*, *119*, 54–61. https://doi.org/10.1016/j.pss.2015.09.013

Yamauchi, M., Lundin, R., Frahm, R. A., Sauvaud, J. A., Holmström, M., & Barabash, S. (2015). Oxygen foreshock of Mars. *Planetary and Space Science*, *119*, 48–53. https://doi.org/10.1016/j.pss.2015.08.003

Yang, Z., Liu, Y. D., Johlander, A., Parks, G. K., Lavraud, B., Lee, E., et al. (2020). MMS direct observations of kinetic-scale shock self-reformation. *The Astrophysical Journal Letters*, *901*(1), L6. https://doi.org/10.3847/2041-8213/abb3ff

Zhang, C., Dong, C., Zhou, H., Deca, J., Xu, S., Harada, Y., et al. (2025). Observational characteristics of electron distributions in the Martian induced Magnetotail. *Geophysical Research Letters*, *52*(7). https://doi.org/10.1029/2024GL113030

Zhang, C., Dong, C., Zhou, H., Halekas, J., Yamauchi, M., Nilsson, H., et al. (2025). Anomalous transient enhancement of planetary ion escape at Mars. *Nature Communications*, *16*(1). https://doi.org/10.1038/s41467-025-58351-y

Zhang, C., Futaana, Y., Nilsson, H., Rong, Z., Persson, M., Klinger, L., et al. (2022). Mars-ward ion flows in the Martian Magnetotail: Mars express observations. *Geophysical Research Letters*, *49*(21). https://doi.org/10.1029/2022gl100691

Zhang, C., Rong, Z., Klinger, L., Nilsson, H., Shi, Z., He, F., et al. (2022). Three-dimensional configuration of induced magnetic fields around Mars. *Journal of Geophysical Research: Planets*, *127*(8). https://doi.org/10.1029/2022je007334